Rayleigh-Taylor instability in accelerated elastic-solid slabs

S. A. Piriz and A. R. Piriz*
Instituto de Investigaciones Energéticas (INEI), E.T.S.I.I., and CYTEMA, Universidad de Castilla-La Mancha, 13071 Ciudad Real, Spain

N. A. Tahir
GSI Helmholtzzentrum für Schwerionenforschung Darmstadt, Planckstrasse 1, 64291 Darmstadt, Germany
(Received 10 July 2017; published 21 December 2017)

We develop the linear theory for the asymptotic growth of the incompressible Rayleigh-Taylor instability of an accelerated solid slab of density ρ_2, shear modulus G, and thickness h, placed over a semi-infinite ideal fluid of density $\rho_1 < \rho_2$. It extends previous results for Atwood number $A_T = 1$ [B. J. Plohr and D. H. Sharp, Z. Angew. Math. Phys. **49**, 786 (1998)] to arbitrary values of A_T and unveil the singular feature of an instability threshold below which the slab is stable for any perturbation wavelength. As a consequence, an accelerated elastic-solid slab is stable if $\rho_2 g h/G \leqslant 2(1 - A_T)/A_T$.

DOI: 10.1103/PhysRevE.96.063115

I. INTRODUCTION

Rayleigh Taylor instability (RTI) is a physical phenomenon well known in fluid mechanics and studied in many different scenarios that develops whenever a heavy fluid lays atop a lighter one or when the light fluid pushes and accelerates the heavier medium [1–22].

RTI is much less understood when it takes place in solid media, although it is of great relevance to geophysical and astrophysical problems, as well as in many experiments on high-energy-density physics and in inertial confinement fusion (ICF).

In fact, in the geophysical framework RTI plays a central role in plate tectonics in which the lithospheric plates sink into Earth's mantle at the subduction zones [23–26]. In astrophysics, it is considered that RTI in an elastic crust could be behind the star quakes taking place in slowly accreting neutron stars and could be responsible for the release of gravitational energy in the form of γ-ray bursts [27–30].

In high-energy-density physics, RTI in solids is present in many laboratory experiments involving the acceleration of solid slabs by means of high explosives [31–34] and intense laser beam [35–37], electrical current [38–40], and ion beam [41–45] pulses. In these investigations RTI is of importance either because it determines the performance of such experiments or because it is used as a tool for assessing mechanical properties of solids submitted to extremely high strains and strain rates.

Besides, in the ICF scenario, the use of a hard solid ablator like Be to control the RTI on the ablation surface is now being examined [46]. A similar approach is being pursued in magnetically driven ICF for the choice of the pusher [47], and it could also be of relevance for the research on ICF driven by ion beams [48].

Despite that in many of the above-mentioned situations the whole RTI evolution will be dependent on the elastic-plastic constitutive properties of the solid slab, the elastic behavior will be dominant at the initial stages of the instability growth [49]. Therefore, the analysis of the RTI in purely elastic solids is also of great importance as a preceding step to the study of more complex situations, including the transition to the plastic regime.

In this regard, the linear regime of RTI in Hookean elastic solids has been theoretically studied in the past mainly by means of approximate models [50–53]. However, only in relatively recent times have these models become reasonably accurate, even though they have typically been restricted to the cases of semi-infinite media and/or Atwood number $A_T = (\rho_2 - \rho_1)/(\rho_2 + \rho_1) = 1$ (where ρ_2 and ρ_1 are, respectively, the densities of the heavy and light media) [33,54–62].

The only exact linear analysis for the incompressible RTI in accelerated elastic-solid slabs were performed by Plohr and Sharp [63] for the particular case of $A_T = 1$ and arbitrary thick slabs, and by Terrones for $A_T \leqslant 1$ in semi-infinite media (solid-solid and solid-fluid interfaces) [64]. The work by Plohr and Sharp applies to the situation of an elastic slab of shear modulus G, density ρ_2, and thickness h, pushed by a constant pressure that produces an acceleration g, so that the top face of the slab is a free surface. This theory predicts that the slab will be stable for the perturbation wave numbers $k \geqslant k_c$, where k_c is a cutoff wave number given by the following implicit equation:

$$\frac{\rho_2 g h}{G} = 2k_c h\left[1 - \left(\frac{k_c h}{\sinh k_c h}\right)^2\right]^{1/2}. \tag{1}$$

In the limit of $kh \ll 1$ the above equation agrees with the results of a previous analytical model for a very thin elastic slab [33,54]. Of course, in the opposite limit, Eq. (1) recovers the cutoff wave number obtained by Terrones (for $A_T = 1$).

This result should be properly distinguished from the outcome of the recent theoretical and experimental work reported by Mora *et al.* for the RTI in a perfectly elastic (Hookean) slab that is hanging from a horizontal rigid wall under the action of the gravity g [65]. For $A_T = 1$, they find the existence of an instability threshold below which the slab is stable for any perturbation wave number, provided that $\rho_2 g h/G \leqslant 6.223$ [65,66] [it is not difficult to see that for $A_T < 1$ this threshold turns out to be $(\rho_2 - \rho_1) g h/G \leqslant 6.223$]. What seems to be a contradiction, as pointed out by Mora *et al.* [65], between this result and the predictions of Eq. (1), reflects

*roberto.piriz@uclm.es

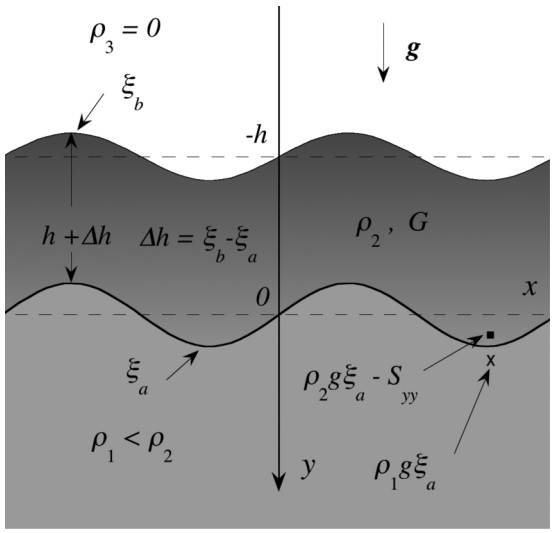

FIG. 1. Schematic of the two-interface system formed by the elastic slab on the top of a semi-infinite ideal fluid.

actually the fact that in their case, a rigid-surface boundary condition applies on the top face of the slab, while Plohr and Sharp consider a free-surface boundary condition, which is more suitable for a slab accelerated by a constant pressure or by a lighter medium.

It may be of interest to mention that the threshold reported by Mora *et al.* has recently been found also for the case of an elastoplastic solid slab. However, in such a case the value of G determining the instability threshold is approximately half of its maximum value (corresponding to very small strains) [67]. Here it is important to remark that this threshold has no relation with the cutoff wave number k_c, although such a cutoff can manifest itself as an instability threshold in experiments in which the finite lateral size of the recipient containing the medium determines a minimum allowed perturbation wave number larger than k_c.

In summary, from the comparison of the results by Plohr and Sharp with those of Refs. [65–67], we should infer that the free-surface boundary condition on the top face of the elastic-solid slab must be responsible for preventing the existence of a threshold for the RTI, at least for the case of $A_T = 1$. However, though the appearance of such an instability threshold when $A_T < 1$ may seem somewhat unexpected, it is possible to demonstrate its existence by using relatively simple physical arguments.

To this end, let us consider an elastic-solid slab of density ρ_2 and shear modulus G laying atop a lighter ideal fluid of density $\rho_1 < \rho_2$. In equilibrium the slab occupies the region $-h \leqslant y \leqslant 0$, and its weight is supported by the ideal fluid below occupying the semispace $y \geqslant 0$, as shown in Fig. 1. When a small perturbation of amplitude ξ_a is applied to the bottom interface at $y = 0$, the top interface at $y = -h$ undergoes a perturbation amplitude ξ_b in such a way that the slab thickens in the valleys by the amount $\Delta h = \xi_a - \xi_b$, so that its weight per unitary surface increases by $\rho_2 g\Delta h$. In addition, just beneath the bottom interface, on the light fluid side, the pressure increases by $\rho_1 g\xi_a$ (Fig. 1).

Therefore, if the slab is unstable for some perturbation wavelength, then it must be $\rho_2 g\Delta h > \rho_1 g\xi_a$. That is, if the slab is unstable, it must undergo a minimum widening $\Delta h = \beta(\rho_1/\rho_2)\xi_a$, with $\beta > 1$, in order to sink into the lighter medium. Such a widening generates an elastic force per unitary surface $S_{yy} \approx 2G\Delta h/h$ on the interface that tends to stabilize it in such a manner that, to keep the perturbation growing, it must be less than the buoyancy force. Namely, $(\rho_2 - \rho_1)g\xi_a > S_{yy}$, and the slab will be unstable if the following condition is satisfied:

$$\frac{\rho_2 gh}{G} > \beta\frac{1 - A_T}{A_T}. \tag{2}$$

In other words, when the condition given by Eq. (2) is not fulfilled, the elastic-solid slab turns out to be stable for any perturbation wavelength, and it determines a threshold for the RTI. We can also notice that for $A_T = 1$ the previous conditions is always satisfied and no threshold exists, in agreement with the results of Refs. [33,63].

In this work we present a formal normal modes analysis for the linear and incompressible RTI taking place in a perfectly elastic-solid slab accelerated by a less dense ideal fluid extending very far from the interface with the slab. For this, the top free-surface boundary condition on the top face of the slab is adopted.

In Sec. II we obtain the linearized equations for the momentum and mass conservation. Thus, in Sec. II A we first obtain the perturbed velocity field by using the Helmholtz decomposition in the rotational and the irrotational parts, which are expressed in terms of potential functions [4,68]. Then we use the Bernoulli gauge to obtain the boundary conditions on both faces of the slab. In Sec. II B these boundary conditions are used to derive the dispersion relation. In Sec. III A the dispersion relation is first solved for the case of zero growth rate in order to get the cutoff wave number beyond which the slab is stable. We also find the instability threshold giving the condition for making the slab stable for any perturbation wavelength. In Sec. III B the growth rate γ is calculated as a function of k, A_T, and h. Concluding remarks are presented in Sec. IV.

II. INSTABILITY LINEAR ANALYSIS

We consider a Hookean solid slab of density ρ_2, thickness h, and shear modulus G that overlays an ideal fluid of density $\rho_1 < \rho_2$ occupying the semispace $y \geqslant 0$. The slab occupies the region $-h \leqslant y \leqslant 0$, and we assume that the region above the slab $y \leqslant -h$ is empty.

The equations for momentum and mass conservation, respectively, read as

$$\rho\frac{d\vec{v}}{dt} = -\vec{\nabla}p + \rho\vec{g} + \vec{\nabla}\cdot\vec{\vec{\sigma}}', \tag{3}$$

$$\frac{d\rho}{dt} + \rho\vec{\nabla}\cdot\vec{v} = 0, \tag{4}$$

where $\vec{v}$, ρ, and p are, respectively, the fluid velocity, density, and pressure; $\vec{g} = g\hat{e}_y = -\vec{\nabla}\varphi$ is the gravity acceleration ($\hat{e}_y$ is the unitary vector in the vertical direction, and φ is the gravitational potential); and $\vec{\vec{\sigma}}'$ is the deviatoric part of the stress tensor $\sigma_{ik} = -p\,\delta_{ik} + \sigma'_{ik}$ (δ_{ik} is the Kronecker δ). For

a Hookean solid, it reads as follows:

$$\frac{\partial \sigma'_{ik}}{\partial t} = G\left(\frac{\partial v_i}{\partial x_k} + \frac{\partial v_k}{\partial x_i}\right). \tag{5}$$

Here, for simplicity, we have switched to the index notation for Cartesian tensors, so that $i = 1,2,3$ indicate, respectively, the space coordinates x, y, z. We will use interchangeably vector and tensor notations for the convenience of the calculations presentation. In addition, dM/dt represents the total material derivative of any magnitude M:

$$\frac{dM}{dt} = \frac{\partial M}{\partial t} + (\vec{v}\cdot\vec{\nabla})M. \tag{6}$$

In order to linearize the previous equations around the equilibrium state, we proceed in the usual manner by writing every magnitude $M\ (\vec{v}, \rho, p, \vec{\vec{\sigma}}')$ as $M = M_0 + \delta M$, where M_0 and $\delta M \ll M_0$ are, respectively, the equilibrium value and the perturbation of M.

Then, for the solid slab in the region $-h \leqslant y \leqslant 0$, we have

$$\rho_2 \frac{\partial(\delta\vec{v}_2)}{\partial t} = -\vec{\nabla}(p_2 + \rho_2\,\delta\varphi_2) + \vec{\nabla}\cdot\vec{\vec{S}}, \tag{7}$$

$$\vec{\nabla}\cdot(\delta\vec{v}_2) = 0, \tag{8}$$

where $S_{ik} \equiv \delta\sigma'_{ik}$, the subindex "2" denotes the solid medium magnitudes, and we have assumed incompressible perturbations ($\delta\rho = 0$).

A. The velocity field

For obtaining the perturbed velocity field we use the Helmholtz decomposition [4,68], and for this we write the velocity field as the sum of an irrotational part $\delta\vec{v}_2^{\,\phi} = \vec{\nabla}\phi_2$, determined by the scalar function ϕ, plus a rotational part $\delta\vec{v}_2^{\,\psi}$ given by the zero divergence vector $\psi_2\hat{e}_z$:

$$\delta\vec{v}_2 = \vec{\nabla}\phi_2 + \vec{\nabla}\times(\psi_2\hat{e}_z). \tag{9}$$

By substituting Eq. (9) into Eq. (8), we find that ϕ_2 must satisfy the Laplace equation:

$$\nabla^2\phi_2 = 0. \tag{10}$$

Similarly, substitution of Eq. (9) into Eq. (7) yields

$$\vec{\nabla}\left(\gamma\phi_2 + \frac{\delta p_2}{\rho_2} + \delta\varphi_2\right) + \vec{\nabla}\times\left[\left(\gamma\psi_2 - \frac{G}{\gamma\rho_2}\nabla^2\psi_2\right)\vec{e}_z\right] = 0, \tag{11}$$

where we have taken $\phi_2 \propto \psi_2 \propto e^{\gamma t}$, with γ being the instability growth rate. As shown in Ref. [4], Eq. (11) can be decoupled by adopting the so-called Bernoulli gauge, for which each term between parentheses must cancel separately:

$$\gamma\phi_2 + \frac{\delta p_2}{\rho_2} + \delta\varphi_2 = 0, \tag{12}$$

$$\gamma^2\psi_2 = \frac{G}{\rho_2}\nabla^2\psi_2. \tag{13}$$

By considering two-dimensional perturbations, we can write $\phi_2 \propto e^{qy}\sin kx$ and $\psi_2 \propto e^{q'y}\cos kx$, and Eqs. (10) and (13) yield, respectively,

$$q = \pm k, \quad q' = \pm\lambda, \quad \lambda = \sqrt{k^2 + \frac{\gamma^2\rho_2}{G}}. \tag{14}$$

Therefore, we can express the potential functions ϕ_2 and ψ_2 in the convenient forms

$$\phi_2 = \frac{a\cosh ky + b\cosh k(h+y)}{\sinh kh}e^{\gamma t}\sin kx, \tag{15}$$

$$\psi_2 = \frac{c\sinh \lambda y + d\sinh \lambda(h+y)}{\sinh \lambda h}e^{\gamma t}\cos kx, \tag{16}$$

and the velocity field is obtained from Eq. (9):

$$\delta v_{2y} = \frac{\partial\phi_2}{\partial y} - \frac{\partial\psi_2}{\partial x}, \quad \delta v_{2x} = \frac{\partial\phi_2}{\partial x} + \frac{\partial\psi_2}{\partial y}. \tag{17}$$

In a similar manner, for the ideal fluid beneath the slab we can write ($y \geqslant 0$)

$$\phi_1 = a_1 e^{-ky}e^{\gamma t}\sin kx, \quad \delta v_{1y} = \frac{\partial\phi_1}{\partial y}, \quad \delta v_{1x} = \frac{\partial\phi_1}{\partial x}, \tag{18}$$

where he subindex "1" denotes the magnitudes in the light ideal fluid.

B. Boundary conditions and dispersion relation

In order to find the instability growth rate γ, we need to impose adequate boundary conditions on the surfaces $y = 0$ and $y = -h$, which will allow for calculating the constants a, b, c, d, and a_1.

1. *Tangential stress continuity at $y = 0$ and $y = -h$*

The tangential stress at these surfaces is given by the perturbation $S_{xy}^{(\nu)}$ of the deviatoric part,

$$S_{xy}^{(\nu)} = \frac{G}{\gamma}\left[\frac{\partial(\delta v_{\nu x})}{\partial y} + \frac{\partial(\delta v_{\nu y})}{\partial x}\right], \tag{19}$$

where $\nu = 1,2,3$ indicates the regions $y \geqslant 0$, $-h \geqslant y \geqslant 0$, and $y \leqslant -h$, respectively. Since region $\nu = 3$ is empty and region $\nu = 1$ is an ideal fluid, these two boundary conditions read

$$S_{xy}^{(2)}(y = 0) = 0, \quad S_{xy}^{(2)}(y = -h) = 0. \tag{20}$$

Then, from Eqs. (15) to (17) we get the following relationships:

$$d = -\frac{2k^2}{\lambda^2 + k^2}b, \quad c = -\frac{2k^2}{\lambda^2 + k^2}a. \tag{21}$$

2. *Normal velocity continuity at $y = 0$*

Normal velocity continuity at $y = 0$ reads as

$$\delta v_{2y}(0) = \delta v_{1y}(0). \tag{22}$$

From Eqs. (15) to (17), it yields

$$a_1 = -(b + d). \tag{23}$$

3. *Normal stress continuity at $y = 0$ and $y = -h$*

The normal stress continuity of $\delta\sigma_{yy}^{(v)} = -\delta p_v + S_{yy}^{(v)}$ is required at both interfaces:

$$-\delta p_2 + S_{yy}^{(2)} = -\delta p_1, \quad \text{at } y = 0, \tag{24}$$

$$-\delta p_2 + S_{yy}^{(2)} = 0, \quad \text{at } y = -h. \tag{25}$$

Then, from Eq. (12) we have

$$-\delta p_2 = \gamma\rho_2\phi_2 - \frac{\rho_2 g\delta v_{2y}}{\gamma}, \tag{26}$$

where we have used that $\delta\varphi_v = -g\eta_v$ and $\dot{\eta}_v = \gamma\eta_v = \delta v_{vy}$.

Therefore, we get an equation for the boundary condition at $y = -h$,

$$\gamma\phi_2 + \frac{2G}{\gamma\rho_2}\frac{\partial(\delta v_{2y})}{\partial y} - \frac{g\delta v_{2y}}{\gamma} = 0, \tag{27}$$

and from Eqs. (15) to (17), it turns out ($y = -h$):

$$\gamma\left(a\coth kh + \frac{b}{\sinh kh}\right) + \frac{2kG}{\gamma\rho_2}\left[k\left(a\coth kh + \frac{b}{\sinh kh}\right) + \lambda\left(c\coth\lambda h + \frac{d}{\sinh\lambda h}\right)\right] + \frac{kg}{\gamma}(a + c) = 0. \tag{28}$$

In a similar manner, the boundary condition at $y = 0$ is written in the form

$$\gamma\phi_2 + \frac{2G}{\gamma\rho_2}\frac{\partial(\delta v_{2y})}{\partial y} - \frac{g\delta v_{2y}}{\gamma} = \frac{\rho_1}{\rho_2}\left(\gamma\phi_1 - \frac{g\delta v_{1y}}{\gamma}\right), \tag{29}$$

and again, from Eqs. (15) to (17), it turns out ($y = 0$)

$$\gamma\left(b\coth kh + \frac{a}{\sinh kh}\right) + \frac{2kG}{\gamma\rho_2}\left[k\left(b\coth kh + \frac{a}{\sinh kh}\right) + \lambda\left(d\coth\lambda h + \frac{c}{\sinh\lambda h}\right)\right] - \frac{kg}{\gamma}(b + d) = \frac{\rho_1}{\rho_2}\left(\gamma + \frac{kg}{\gamma}\right)a_1. \tag{30}$$

4. *Dispersion relation*

The set formed by Eqs. (21), (23), (28), and (30) can be written in a more compact form as

$$a(C + B) + bA = 0, \tag{31}$$

$$aA + b\left[C - B + \frac{\rho_1}{\rho_2}\left(B + \frac{\gamma^2\rho_2}{G}\right)\right] = 0, \tag{32}$$

where $B = \rho_2 kg/G$, and A and C are defined as in Ref. [63]:

$$A = \frac{(\lambda^2 + k^2)^2\,\mathrm{csch}\,kh - 4k^3\lambda\,\mathrm{csch}\,\lambda h}{\lambda^2 - k^2}, \tag{33}$$

$$C = \frac{(\lambda^2 + k^2)^2\coth kh - 4k^3\lambda\coth\lambda h}{\lambda^2 - k^2}. \tag{34}$$

As expected, Eqs. (31) and (32) reduce to the system obtained in Ref. [63] for $\rho_1 = 0$. Then, from the condition that the determinant of such a system must be equal to zero, we obtain the following dispersion relation:

$$C^2 - A^2 = B^2 - \frac{\rho_1}{\rho_2}(C + B)\left(B + \frac{\gamma^2\rho_2}{G}\right). \tag{35}$$

III. THEORY RESULTS

A. Cutoff wave number and instability threshold

Since we expect a cutoff wave number k_c above which the slab becomes stable [33–64], we start by solving Eq. (35) for the particular case of $\gamma = 0$. Then, by using the L'Hôpital rule, we get expressions for A and C at $\gamma = 0$ ($k = k_c$),

$$A = \frac{2k_c^2(k_c h\cosh k_c h + \sinh k_c h)}{\sinh^2 k_c h}, \tag{36}$$

$$C = \frac{k_c^2(2k_c h + \sinh 2k_c h)}{\sinh^2 k_c h}, \tag{37}$$

and Eq. (35) for $\gamma = 0$ turns out

$$\frac{2A_T}{1 + A_T}\alpha^2 - \frac{1 - A_T}{1 + A_T}\frac{w(2w + \sinh 2w)}{\sinh^2 w}\alpha - 4w^2\left[1 - \left(\frac{w}{\sinh w}\right)^2\right] = 0, \tag{38}$$

where $\alpha = \rho_2 gh/G \equiv k_0 h$ ($k_0 = \rho_2 g/G$) and $w = k_c h$.

We have represented $\alpha(w)$ for different values of the Atwood number A_T in Fig. 2(a), where we can see that it has a minimum value $\alpha^* = 2(1 - A_T)/A_T$, indicating the instability threshold below which the slab is stable for all the perturbation wavelengths. The analytical expression of this threshold is easily obtained from Eq. (38) by taking the limit $w \ll 1$.

Figure 2(b) shows the dimensionless cutoff wave number $\kappa_c = k_c/k_0 = w/\alpha$ as a function of the dimensionless thickness $\alpha = k_0 h$ of the slab. For all the values of A_T, the normalized cutoff wave number $(1 + A_T)\kappa_c/A_T$ follows the same behavior as for the case with $A_T = 1$ provided that α is well above the threshold value α^* ($\alpha \gtrsim 1.5$ to $3\alpha^*$, depending on A_T). Then, it decreases and drops suddenly to zero for $\alpha = \alpha^*$.

In conclusion, for $\alpha < 2(1 - A_T)/A_T$, the elastic slab is stable for any perturbation wavelength, such as it was qualitatively discussed in Sec. I [Eq. (2) with $\beta = 2$].

B. Instability growth rate

We can calculate the instability growth rate γ as a function of the perturbation wave number k, with the Atwood number A_T and the slab thickness h as parameters. For this, it is convenient first to use the following dimensionless magnitudes:

$$\kappa = \frac{k}{k_0}, \quad \sigma = \frac{\gamma}{\sqrt{k_0 g}}, \quad k_0 = \frac{\rho_2 g}{G}. \tag{39}$$

After some somewhat tedious but straightforward algebra, we get the following equation for the dimensionless growth

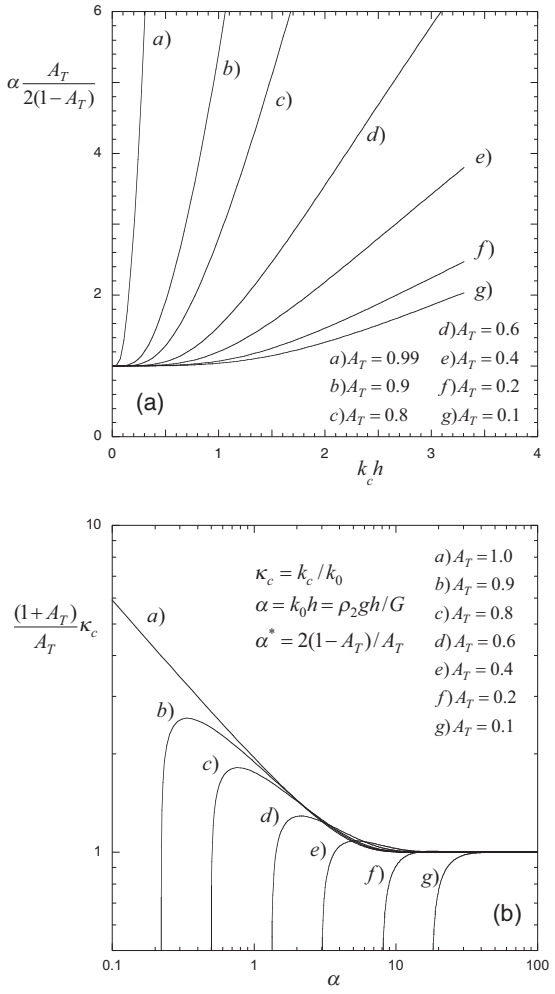

FIG. 2. (a) Slab thickness $\alpha = k_0 h$ as a function of the cutoff wave number $w = k_c h$ for several values of the Atwood number A_T. (b) Normalized cutoff wave number $(1 + A_T)\kappa_c / A_T$ ($\kappa_c = k_c / k_0 = w/\alpha$) as a function of the dimensionless slab thickness $\alpha = k_0 h$ for several values of A_T.

rate σ:

$$(2\kappa^2 + \sigma^2)^4 + 16\kappa^6(\sigma^2 + \kappa^2) - 8\kappa^3\sqrt{\sigma^2 + \kappa^2}(2\kappa^2 + \sigma^2)^2 \times (\coth \alpha\kappa \coth \alpha\sqrt{\sigma^2+\kappa^2} - \operatorname{csch} \alpha\kappa \operatorname{csch} \alpha\sqrt{\sigma^2+\kappa^2}) = \kappa^2\sigma^4 - \frac{1 - A_T}{1 + A_T}\sigma^2(\kappa^2 + \sigma^2)[\kappa + (2\kappa^2 + \sigma^2)^2 \coth \alpha\kappa - 4\kappa^3\sqrt{\sigma^2+\kappa^2} \coth \alpha\sqrt{\sigma^2+\kappa^2}]. \quad (40)$$

As for the case with $A_T = 1$ [63], this is a biquartic transcendental equation for σ as a function of κ, with the parameters A_T and α, and it can be shown to have a unique real and positive root for any value of the arguments when the slab is unstable.

We have represented $\sigma(\kappa)$ in Fig. 3 for three different Atwood numbers ($A_T = 1, 0.8$, and 0.4) and for several values of the dimensionless thickness α larger than the threshold value α^*. In Fig. 3(a) we show the case for $A_T = 1$, already presented in Ref. [63]. As it was discussed in Ref. [69], the growth rate is independent of the slab thickness for the smallest

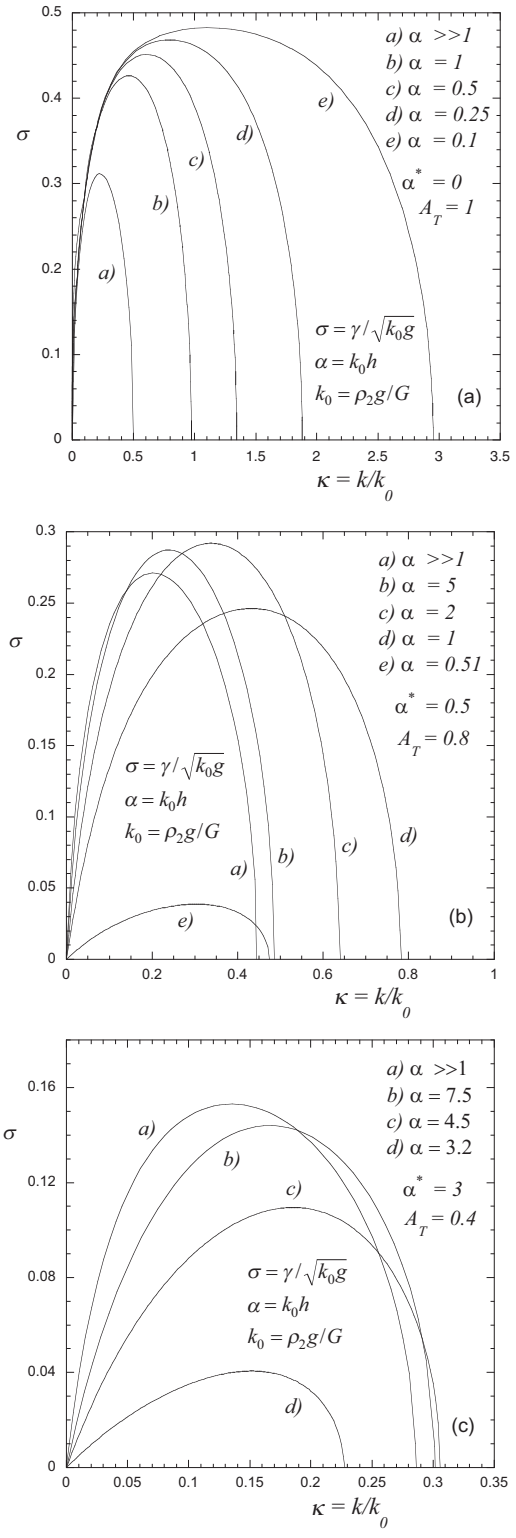

FIG. 3. Asymptotic growth rate $\sigma = \gamma / \sqrt{k_0 g}$ as a function of the wave number $\kappa = k/k_0$ for several values of $\alpha = k_0 h$ and for (a) $A_T = 1$, (b) $A_T = 0.8$, and (c) $A_T = 0.4$.

perturbation wave numbers κ when the elasticity effects are not yet important, in agreement with the corresponding results for an ideal-fluid slab ($G = 0$). In fact, for such a case, Eq. (40) reduces to the well-known result obtained first by Taylor,

which for $A_T = 1$ yields the classical growth rate [2,20]:

$$\sigma^2 = \frac{2A_T\kappa}{1 + A_T + (1 - A_T)\coth \alpha\kappa}. \tag{41}$$

Then, when κ increases the elastic force provides the stabilization that reduces the growth rate and makes it equal to zero for $\kappa = \kappa_c$. However, we can see in Fig. 3(a) that the stabilizing effect of the elasticity becomes less effective as the slab becomes thinner, and this is because the elastic force is actually determined by the total strain across the slab thickness rather than by the local strain on the slab interfaces [69]. Therefore, since the local strain becomes more uniform through the slab thickness for the thinner slabs, the total strain decreases and the stabilizing elastic force is reduced.

Such a behavior persists for $A_T < 1$ as far as the dimensionless thickness α is appreciably larger than the threshold value α^* [Fig. 3(b)]. In such a case, the growth rate for the smallest wave numbers is smaller for thinner slabs for which the stabilizing effect of the slab thickness observed for an ideal fluid still prevails [Eq. (41)]. Again, though, when κ increases, the loss of the elasticity effectiveness starts to make the thicker slabs more stable [curves (a), (b), and (c) of Fig. 3(b)]. However, the existence of the instability threshold for $A_T < 1$ finally leads to a sudden increase of the elastic force as α approaches the threshold value α^*, producing a strong reduction of the growth rate [curves (d) and (e) of Fig. 3(b)], which eventually becomes null for $\alpha = \alpha^*$. Such a behavior is more evident for smaller values of A_T [Fig. 3(c)].

As was qualitatively discussed in Sec. I, the increase of the elastic force for the thinnest slabs (when $A_T < 1$) is the consequence of the minimum total strain $\Delta h/h$ necessary to sustain the instability growth, which not only prevents the further reduction of the elastic force but produces a sudden increase of it as the slab becomes thinner. This effect is absent when $A_T = 1$ when no minimum value of Δh exists, and it is instead stronger for smaller values of A_T for which α^* becomes larger.

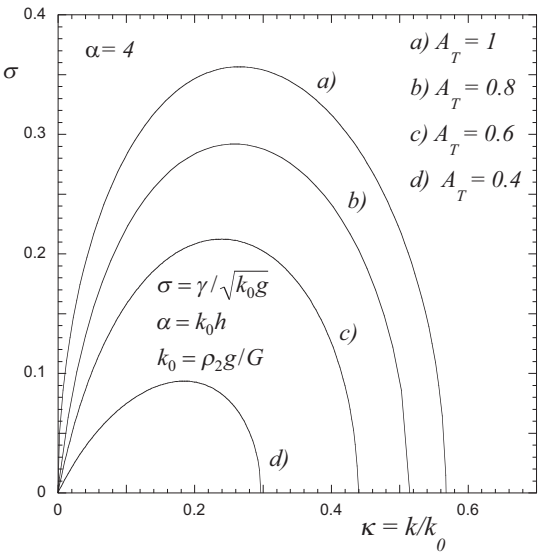

FIG. 4. Growth rate $\sigma = \gamma/\sqrt{k_0 g}$ as a function of the wave number $\kappa = k/k_0$ for several values of A_T and $\alpha = k_0 h = 4$.

In Fig. 4 we show the effect of changing the Atwood number for a fixed value of $\alpha > \alpha^*$ (for all the values of A_T). In this case the instability growth rate decreases with A_T such as can be expected.

Finally, it may be worth mentioning that in Eq. (40) σ^2 always is a real number, so the onset of instability oscillatory motions (overstability) does not occur, such as is typical in other RTI-related problems. We have checked this condition in all our calculations presented in Figs. 2 to 4. However, a mathematically rigorous demonstration valid also for the present case with arbitrary values of A_T can be found in Ref. [67] (see also Ref. [70] for a similar conclusion on RTI in viscous fluids).

IV. CONCLUDING REMARKS

We have developed the linear theory for two-dimensional perturbations of the incompressible RTI of an elastic-solid slab overlaying a semi-infinite ideal fluid. This extends the previous work by Plohr and Sharp [63] for $A_T = 1$, to arbitrary values of the Atwood number.

A singular feature is found that shows the existence of a threshold for the occurrence of the instability, according to which the relatively thinner slabs are stable for any perturbation wavelength. This characteristic of RTI in elastic solids, at first glance unexpected, can, however, be demonstrated on the basis of qualitative physical arguments.

It represents the corresponding counterpart for slabs with a top free surface, to the instability threshold recently reported for elastic-solid slabs with a top rigid surface [65–67]. However, it represents an important advance in the understanding of RTI in solids for situations of interest in many research fields in which the top free-surface boundary condition represents a more realistic description of the physical situation.

In particular, it is expected to have an impact on the design of laboratory experiments on high-energy-density physics in which it should also affect the stability region of an elastic-plastic solid slab [49,57]. In fact, if the transition to the plastic regime occurs for relatively thin solid slab being below the threshold, the instability condition would be ruled only by the yield strength in a manner similar to the one stipulated by the Drucker criterion on the initial perturbation amplitude [49,71,72].

In the design of the Laboratory of Planetary Sciences (LAPLAS) experimental setup, planned at the GSI Helmholtzzentrum für Schwerionenforschung in Darmstadt, Germany, for the research on high-energy-density physics in the framework of the Facility for Antiproton and Ion Research (FAIR), a cylindrical shell with a W pusher ($G = 160$ GPa, $\rho_2 = 19.3$ g/cm^3) is imploded by heating the surrounding region (the absorber) by means of an intense ion beam pulse with an annular focal spot. The absorber is also made of the same heavy material, and it is tamped to avoid the outwards expansion so that typical pressures $p_0 = \rho_2 g h$ of about 2 Mbar are generated for pushing and accelerating the solid pusher. The numerical simulations show that the pusher remains in solid state and that the condition $\alpha < \alpha^*$ is always satisfied during the implosion process [73]. Then, the implosion stability would be assured provided that a symmetry

level (determined by the yield strength of the pusher) better than 1% is achieved [41,42,44,45].

Experiments with high explosives could also take advantage of the instability threshold by designing them with slab materials having the highest shear modulus and using explosives with densities as high as possible to drive the slab acceleration, so that A_T remains reasonable small during the whole process [31–33].

In inertial confinement fusion, it has been recently reported that in order to control the RT instability and to achieve ignition, it may be necessary to use a hard solid ablator (Be) to drive the ablative implosion and keep it below the melting curve [46]. Since the ablation process determines a density gradient of the ablated plasma, an effective Atwood number will be defined for every perturbation wave number [18–22]. Therefore, the instability threshold we have described here would set a new cutoff wave number, associated with the ablator shear modulus G, competing with the classical ablative cutoff wave number.

To conclude, it may be of interest to make a short comment about some limits of the validity of the present theory.

In the first place, we have assumed that perturbations are imposed on an equilibrium situation consisting of a purely elastic layer laying atop a semi-infinite ideal fluid. The physical realization of this configuration requires that the hydrostatic pressure $\rho_2 gh$ be less than the yield strength Y that determines the elastic limit beyond which Hooke's law is not applicable any longer, and the transition to a plastic regime takes place [49–53,57–62,74–76]. Since it is typically $Y \sim 0.01G$, the slab would be perfectly stable for practically any Atwood number less than 1 [Eq. (2)].

Instead, if during the instability evolution this hydrostatic pressure increases with time beyond the elastic limit, then a transition to the plastic regime will take place. Although the analysis of such situation is beyond the scope of the present work, if the pressure remains below the threshold given by Eq. (2), we can speculate on the basis of the results of Ref. [49] that the stability boundary will be determined only by Drucker' criterion on the perturbation amplitude [49,71,72], independently of the particular perturbation wavelength, provided that we remain in the linear regime. However, more research is necessary in order to completely understand this elastic-plastic transition.

Another discussion that may be pertinent regards the incompressible linear analysis we have performed. We have just assumed that density perturbation can be neglected ($\delta\rho = 0$), and we have not addressed the hydrostatic equilibrium configuration which will be determined by the particular equation of state of the media. The previous condition of incompressible perturbations requires that the characteristic velocity γ/k be less than the sound speed c_s in the solid slab. Introducing the dimensionless magnitudes defined in Eq. (39), we have $(\sigma/\kappa)^2 G/(\rho_2 c_2^2) < 1$, a condition that is well satisfied in most of practical situations for the whole range of unstable perturbation wave numbers considered in Figs. 3 and 4.

Regarding the hydrostatic equilibrium, the particular equation of state will determine density profiles $\rho(y)$ within the media, which we have not considered in order to keep the theory as simple as possible. Although strong gradients are not expected in the solid slab, they will have some effect on the instability growth rate. However, such effects do not represent any serious limitation to the present theory since density gradients could be taken into account in an approximate manner by considering an effective Atwood number defined by the local values of the density on each side of the interface at a distance of the order of k^{-1}, or h (whatever is the smallest one in the solid slab), from the interface: $\rho_1 = \rho(y = k^{-1})$, and $\rho_2 = \rho(y = -y_{\min})$, where $y_{\min}$ is smallest between k^{-1} and h. Such a procedure provides a quick evaluation of the gradient effects, and it is known to yield pretty good results [22,77].

ACKNOWLEDGMENTS

This work has been partially supported by the Ministerio de Economía y Competitividad of Spain (Grants No. ENE2013-45661-C2-1-P and No. ENE2016-75703-R) and by the BMBF of Germany.

[1] L. Rayleigh, *Scientific Papers* (Cambridge University Press, Cambridge, UK, 1900), Vol. II, pp. 200–207.
[2] G. I. Taylor, Proc. R. Soc. London, Ser. A **201**, 192 (1950).
[3] S. Chandrasekhar, *Hydrodynamics and Hydromagnetic Stability* (Dover, New York, 1961), pp. 428–480.
[4] R. Menikoff, R. C. Mjolness, D. H. Sharp, C. Zemach, and B. J. Doyle, Phys. Fluids **21**, 1674 (1978).
[5] D. H. Sharp, Phys. D (Amsterdam, Neth.) **12**, 3 (1984).
[6] H. J. Kull, Phys. Rep. **206**, 197 (1991).
[7] N. A. Inogamov, Astrophys. Space Phys. **10**, 1 (1999).
[8] K. O. Mikaelian, Phys. Rev. A **26**, 2140 (1982).
[9] K. O. Mikaelian, Phys. Rev. A **28**, 1637 (1983).
[10] K. O. Mikaelian, Phys. Rev. E **54**, 3676 (1996).
[11] K. O. Mikaelian, Phys. Rev. A **42**, 7211 (1990).
[12] A. R. Piriz, O. D. Cortazar, J. J. L. Cela, and N. A. Tahir, Am. J. Phys. **74**, 1095 (2006).
[13] Y. Y. Lau, J. C. Zier, I. M. Rittersdorf, M. R. Weis, and R. M. Gilgenbach, Phys. Rev. E **83**, 066405 (2011).
[14] M. R. Weis, P. Zhang, Y. Y. Lau, I. M. Rittersdorf, J. C. Zier, R. M. Gilgenbach, M. H. Hess, and K. J. Peterson, Phys. Plasmas **21**, 122708 (2014).
[15] M. S. Plesset and C. G. Whipple, Phys. Fluids **17**, 1 (1974).
[16] W. Harrison, Proc. London Math. Soc. **s2**, 396 (1908).
[17] S. Parhi and G. Nath, Int. J. Eng. Sci. **29**, 1439 (1991).
[18] R. Betti, V. N. Goncharov, R. L. McCrory, and C. P. Verdon, Phys. Plasmas **2**, 3844 (1995).
[19] V. N. Goncharov, R. Betti, R. L. McCrory, P. Sorotokin, and C. P. Verdon, Phys. Plasmas **3**, 1402 (1996).

[20] V. N. Goncharov, P. McKenty, S. Skupsky, R. Betti, R. L. McCrory, and C. Cherfils-Clérouin, Phys. Plasmas **7**, 5118 (2000).

[21] J. G. Wouchuk and A. R. Piriz, Phys. Plasmas **2**, 493 (1995).

[22] A. R. Piriz, J. Sanz, and L. F. Ibañez, Phys. Plasmas **4**, 1117 (1997).

[23] E. B. Burov and P. Molnar, Earth Planet. Sci. Lett. **275**, 370 (2008).

[24] W. Gorczyk, B. Gobbs, and T. Gerya, Tectonophysics **514**, 146 (2012).

[25] W. Gorczyk and K. Vogt, Gondwana Res. **27**, 196 (2015).

[26] S. L. Shapiro and S. A. Teukolsky, *Black Holes, White Dwarfs, and Neutron Stars. The Physics of Compact Objects* (Wiley-VCH, Weinheim, Germany, 2004).

[27] O. Blaes, R. Blandford, P. D. Madau, and P. Koonin, Astrophys. J. **363**, 612 (1990).

[28] O. Blaes, R. Blandford, P. D. Madau, and L. Yan, Astrophys. J. **399**, 634 (1992).

[29] P. C. Mock and P. C. Joss, Astrophys. J. **500**, 374 (1998).

[30] D. Kobyakov and C. J. Pethick, Phys. Rev. Lett. **112**, 112504 (2014).

[31] J. F. Barnes, P. J. Blewet, R. G. McQueen, K. A. Meyer, and D. Venable, J. Appl. Phys. **45**, 727 (1974).

[32] J. F. Barnes, D. H. Janney, R. K. London, K. A. Meyer, and D. H. Sharp, J. Appl. Phys. **51**, 4678 (1980).

[33] S. M. Bakhrakh, O. B. Drennov, N. P. Kovalev, A. I. Lebedev, E. E. Meshkov, A. L. Mikhailov, N. V. Neumerzhitsky, P. N. Nizovtsev, V. A. Rayevsky, G. P. Simonov, V. P. Solovyev, and I. G. Zhidov, Lawrence Livermore National Laboratory Report No. UCRL-CR-126710, 1997 (unpublished); available at https://www.osti.gov/scitech/servlets/purl/515973

[34] D. H. Kalantar, B. A. Remington, J. D. Colvin, K. O. Mikaelian, S. V. Weber, L. G. Wiley, J. S. Wark, A. Loveridge, A. M. Allen, A. A. Hauer, and M. A. Meyers, Phys. Plasmas **7**, 1999 (2000).

[35] B. A. Remington, P. Allen, E. M. Bringa, J. Hawreliak, D. Ho, K. T. Lorenz, H. Lorenzana, J. M. McNaney, M. A. Meyers, S. W. Pollaine, K. Rosolankova, B. Sadik, M. S. Schneider, D. Swift, J. Wark, and B. Yaakobi, Mater. Sci. Tech. **22**, 474 (2006).

[36] H.-S. Park, K. T. Lorenz, R. M. Cavallo, S. M. Pollaine, S. T. Prisbrey, R. E. Rudd, R. C. Becker, J. V. Bernier, and B. A. Remington, Phys. Rev. Lett. **104**, 135504 (2010).

[37] A. R. Piriz, J. J. L. Cela, and N. A. Tahir, Phys. Rev. Lett. **105**, 179601 (2010).

[38] R. E. Reinovsky, W. E. Anderson, W. L. Atchison, C. E. Ekdahl, R. J. Faehl, I. R. Lindemuth, D. V. Morgan, M. Murillo, J. L. Stokes, and J. S. Shlachter, IEEE Trans. Plasma Sci. **30**, 1764 (2002).

[39] D. B. Sinars *et al.*, Phys. Rev. Lett. **105**, 185001 (2010).

[40] R. D. McBride *et al.*, Phys. Plasmas **20**, 056309 (2013).

[41] J. J. López Cela, A. R. Piriz, M. C. Serna Moreno, and N. A. Tahir, Laser Part. Beams **24**, 427 (2006).

[42] N. A. Tahir, A. Shutov, I. V. Lomonosov, A. R. Piriz, G. Wouchuk, C. Deutsch, D. H. H. Hoffmann, and V. E. Fortov, High Energy Density Phys. **2**, 21 (2006).

[43] N. A. Tahir, V. Kim, A. Matvechev, A. Ostrik, A. V. Shutov, I. V. Lomonosov, A. R. Piriz, J. J. L. Cela, and D. H. H. Hoffmann, Nucl. Instrum. Methods Phys. Res., Sect. B **245**, 85 (2006).

[44] N. A. Tahir, P. Spiller, A Shutov, I. V. Lomonosov, V. Gryaznov, A. R. Piriz, G. Wouchuk, C. Deutsch, F. Fortov, D. H. H. Hoffmann, and R. Schmidt, Nucl. Instrum. Methods Phys. Res., Sect. A **577**, 238 (2007).

[45] N. A. Tahir, C. Deutsch, V. E. Fortov, V. Gryaznov, D. H. H. Hoffmann, M. Kulish, I. V. Lomonosov, V. Mintsev, P. Ni, D. Nikolaev, A. R. Piriz, N. Shilkin, P. Spiller, A. Shutov, M. Temporal, V. Ternovoi, S. Udrea, and D. Varentsov, Phys. Rev. Lett. **95**, 035001 (2005).

[46] S. Opie, E. Loomis, P. Peralta, T. Shimada, and R. P. Johnson, Phys. Rev. Lett. **118**, 195501 (2017).

[47] P. F. Knapp, M. R. Martin, D. H. Dolan, K. Cochrane, D. Dalton, J.-P. Davis, C. A. Jennings, G. P. Loisel, D. H. Romero, I. C. Smith, E. P. Yu, M. R. Weis, T. R. Mattsson, R. D. McBride, K. Peterson, J. Schwarz, and D. B. Sinars, Phys. Plasmas **24**, 042708 (2017).

[48] A. R. Piriz, Phys. Fluids **31**, 658 (1988).

[49] A. R. Piriz, J. J. L. Cela, and N. A. Tahir, Phys. Rev. E **80**, 046305 (2009).

[50] J. W. Miles, General Dynamics Report No. GAMD-7335, AD 643161, 1966 (unpublished).

[51] G. N. White, Los Alamos National Laboratory Report No. LA-5225-MS, 1973 (unpublished).

[52] A. C. Robinson and J. W. Swegle, J. Appl. Phys. **66**, 2859 (1989).

[53] E. L. Ruden and D. E. Bell, J. Appl. Phys. **82**, 163 (1997).

[54] A. I. Lebedev, P. N. Nisovtsev, and V. A. Rayevsky, in *Proceedings of the 4th International Workshop on the Physics of Compressible Turbulent Mixing (IWPCTM), 29 March-1 April 1993, Cambridge, England* (Cambridge University Press, New York, 1993), p. 81.

[55] A. R. Piriz, J. J. L. Cela, O. D. Cortazar, N. A. Tahir, and D. H. H. Hoffmann, Phys. Rev. E **72**, 056313 (2005).

[56] A. R. Piriz, J. J. L. Cela, N. A. Tahir, and D. H. H. Hoffmann, Phys. Rev. E **74**, 037301 (2006).

[57] A. R. Piriz, J. J. L. Cela, and N. A. Tahir, J. Appl. Phys. **105**, 116101 (2009).

[58] A. R. Piriz, Y. B. Sun, and N. A. Tahir, Phys. Rev. E **88**, 023026 (2013).

[59] A. R. Piriz, Y. B. Sun, and N. A. Tahir, Phys. Rev. E **89**, 063022 (2014).

[60] Y. B. Sun and A. R. Piriz, Phys. Plasmas **21**, 072708 (2014).

[61] A. R. Piriz, Y. B. Sun, and N. A. Tahir, Eur. J. Phys. **38**, 015003 (2017).

[62] A. R. Piriz, Y. B. Sun, and N. A. Tahir, Phys. Rev. E **91**, 033007 (2015).

[63] B. J. Plohr and D. H. Sharp, Z. Angew. Math. Phys. **49**, 786 (1998).

[64] G. Terrones, Phys. Rev. E **71**, 036306 (2005).

[65] S. Mora, T. Phou, J.-M. Fromental, and Y. Pomeau, Phys. Rev. Lett. **113**, 178301 (2014).

[66] D. Riccobelli and P. Ciarletta, Philos. Trans. R. Soc., A **375**, 20160421 (2017).

[67] I. Maimouni, J. Goyon, E. Lac, T. Pringuey, J. Boujlel, X. Chateau, and P. Coussot, Phys. Rev. Lett. **116**, 154502 (2016).

[68] H. Lamb, *Hydrodynamics* (Dover, Mineola, NY, 1945).

[69] S. A. Piriz, A. R. Piriz, and N. A. Tahir, Phys. Rev. E **95**, 053108 (2017). In the analysis presented in the Appendix

B, some calculation mistakes were made that prevented the unveiling of the existence of the instability threshold for $A_T < 1$. The existence of this threshold limits the model validity to large values of A_T or values of α well above the threshold.

[70] A. Pellew and R. V. Southwell, Proc. R. Soc. London, Ser. A **176**, 312 (1940).

[71] D. C. Drucker, in *Mechanics Today*, edited by S. Nemmat-Nasser Pergamon Pergamon, Oxford, UK, (1980), Vol. 5, p. 37.

[72] D. C. Drucker, Ing.-Arch. **49**, 361 (1980).

[73] N. A. Tahir, I. V. Lomonosov, B. Borm, A. R. Piriz, A. Shutov, P. Neumayer, V. Bagnoud, and S. A. Piriz, Astrophys. J. Suppl. Ser. **232**, 1 (2017).

[74] A. R. Piriz, J. J. L. Cela, N. A. Tahir, and D. H. H. Hoffmann, Phys. Rev. E **78**, 056401 (2008).

[75] V. V. Zhakhovskii and N. A. Inogamov, JETP Lett. **92**, 521 (2010).

[76] V. V. Zhakhovsky, M. M. Budzevich, N. A. Inogamov, I. I. Oleynik, and C. T. White, Phys. Rev. Lett. **107**, 135502 (2011).

[77] J. Lindl, Phys. Plasmas **2**, 3933 (1995).